AIP | Journal of Applied Physics

# Configuration interaction approach to Fermi liquid–Wigner crystal mixed phases in semiconductor nanodumbbells

A. Ballester, J. L. Movilla, J. M. Escartín, M. Pi, and J. Planelles

Citation: J. Appl. Phys. **112**, 024311 (2012); doi: 10.1063/1.4737774
View online: http://dx.doi.org/10.1063/1.4737774
View Table of Contents: http://jap.aip.org/resource/1/JAPIAU/v112/i2
Published by the American Institute of Physics.

# Configuration interaction approach to Fermi liquid–Wigner crystal mixed phases in semiconductor nanodumbbells

A. Ballester,[1] J. L. Movilla,[1] J. M. Escartín,[2,3] M. Pi,[4] and J. Planelles[1,a)]
[1]*Departament de Química Física i Analítica, Universitat Jaume I, Box 224, E-12080 Castelló, Spain*
[2]*CNRS, UMR 5152, 31062 Toulouse Cedex 4, France*
[3]*Laboratoire de Physique Théorique, IRSAMC, Université de Toulouse, UPS, 31062 Toulouse Cedex 4, France*
[4]*Departament ECM, Facultat de Física, and IN2UB, Universitat de Barcelona, E-08028 Barcelona, Spain*

(Received 8 May 2012; accepted 20 June 2012; published online 20 July 2012)

Full configuration interaction calculations demonstrate the existence of mixed correlation phases in truly three-dimensional elongated nanocrystals subject to inhomogeneous spatial confining potentials. In such phases, the electron density behaves like a Fermi liquid in some regions, while, simultaneously, other more dilute regions display the typical quasi-classical Wigner distribution. The present results confirm and strengthen previous local spin-density functional theory predictions [Ballester *et al.*, Phys. Rev. B **82**, 115405 (2010)]. Additionally, simulation of the in-plane and *z*-polarized modes of the absorption spectra reveals the different correlation regimes occurring in these systems. © *2012 American Institute of Physics*. [http://dx.doi.org/10.1063/1.4737774]

## I. INTRODUCTION

Semiconductor quantum dots (QD) have been an active field of research in chemistry, materials science, and solid state physics over the last decades.[1] The interest of these structures arises from their atomic-like behavior, i.e., discrete energy spectrum and finite number of confined carriers, along with the possibility of tuning their behavior artificially by changing the dimensions and the composition of the dots. This flexibility has made it possible to investigate systems with atomic-like response in physical regimes, which are unattainable for natural atoms. The gain in basic science this has brought about has allowed researchers to envisage new technological devices, which were inconceivable a few years ago. The practical development of these devices, in turn, has opened new theoretical and experimental challenges.

Dependence of nanocrystal properties on size and shape has been investigated, thanks to successful control of growth during experimental synthesis.[2] In particular, colloidal elongated quantum dots are of theoretical interest due to their anisotropic spatial confinement. These nanosystems represent the transition from spherical to rod-like shape with a preferential growth direction. The relaxation of the spatial confinement along the longitudinal direction leads to a weak confinement regime, in which the electronic correlations may play an important role. As a consequence, anisotropic shape confers different properties to nanorods as compared to their spherical counterpart. Thus, depending on the dimensions of nanorods, the band gap[3] and the optical properties[4] are modified.

In addition to size and shape, heterogeneous composition introduces new structural effects. Nowadays, mixed-semiconductor heterostructures are synthesized[5] with precise shapes. In particular, CdSe/CdTe heterojunctions yield structures composed of a nanorod sandwiched between two spherical caps. This structure is referred to as nanobarbell or nanodumbbell (ND)[6] and presents an inhomogeneous confining potential and promising technological applications.[7]

Among the exotic physical regimes difficult to attain in natural atoms but straightforwardly reachable in artificial heterostructures, we may mention the Wigner crystal. In 1934 Wigner predicted that, below a critical electron density, the electron gas crystallizes and forms a lattice of electrons arranged in precise classical configurations.[8] This is due to the fact that the kinetic energy becomes negligible relative to the Coulomb energy so that correlations dominate the electronic structure. Many classical electron configurations in artificial structures have been reported up to date (see, e.g., Refs. 9 and 10). In contrast, crystallization processes in the presence of highly inhomogeneous potentials seem to have attracted much less attention.[11–13]

In a recent paper,[14] local spin-density functional theory (LSDFT) calculations demonstrated the existence of mixed phases (MPs) in CdSe/CdTe/CdSe NDs, driven by the inhomogeneous spatial confining potentials. In a MP the electron density behaves like a standard Fermi liquid in some regions while, simultaneously, other more dilute regions display the profile of a typical Wigner crystal.

In this article, we carry out full configuration interaction (FCI) calculations of the ground and lowest-lying excited states of many electrons confined in a CdSe/CdTe/CdSe ND. We identify the formation of MPs in the ground states, thus confirming and reinforcing the previous results obtained at the LSDFT level. Additionally, we carry out the simulations of absorption spectra to find out fingerprints and thus probe the different correlation regimes occurring in the MPs of these systems.

## II. THEORY AND MODELS

We study MPs in CdSe/CdTe/CdSe NDs. The ND model is built by attaching two $R = 2.2$ nm radius spherical

a)Author to whom correspondence should be addressed. Electronic mail: josep.planelles@qfa.uji.es.

 

CdSe caps to the tips of a CdTe cylinder of radius $R=2\,\text{nm}$ and length $L=55\,\text{nm}$, as depicted in Fig. 1. We have previously studied this system at the LSDFT level and found the existence of MPs in the system.[14] A twofold reason leads us to choose the employed materials. On the one hand, they are materials used nowadays in many syntheses of elongated nanocrystals,[5,6,15] and, on the other hand, they have a rather large band offset but very similar effective masses and dielectric constants, so that no relevant effects coming from effective mass and/or dielectric constant inhomogeneities will mask those coming from an inhomogeneous confining potential derived from the band offset. The isotropic and uniform electron effective mass, $m^*=0.13$, and dielectric constant, $\epsilon=9.2$, employed in our models are those of bulk material.[16] We assume the 0.42 eV CdSe/CdTe conduction band offset[17] as the confining barrier height between these materials, and set the origin of energies at the bottom of the CdTe conduction band. Since no specific QD environment is determined, we assume a typical 4 eV confining QD-environment barrier (see Fig. 1).

The Hamiltonian (in a.u.) of an electron confined in this ND reads as follows:

$$\hat{h}_i=-\frac{1}{2m^*}\nabla_i^2+V_i^c \tag{1}$$

with $V_i^c$ standing for the spatial confining potential (see Fig. 1(b)). Therefore, the many-electron Hamiltonian for the system results

$$\hat{H}=\sum_{i=1}^{N}\hat{h}_i+\sum_{i<j}^{N}\frac{1}{\epsilon}\frac{1}{|\mathbf{r}_i-\mathbf{r}_j|}, \tag{2}$$

where $N$ is the number of electrons.

The many-electron Hamiltonian equation (2) is solved variationally by means of a FCI approach. To this end, we employ the CI code available at the address given in Ref. 18. In order to carry out the FCI calculation, one first has to select a given finite $M$-dimensional one-electron basis set $\{\phi_p\}_{p=1}^{M}$ and then build all possible $N$-body Slater determinants $\Phi_i=\det\{\phi_1\phi_2\ldots\phi_N\}$ out of them. In a second step, the projection of Hamiltonian (2) onto the basis set of Slater determinants is carried out, yielding matrix elements $\langle\Phi_i|\hat{H}|\Phi_j\rangle$ (one may eventually select a subset of spin- and symmetry-adapted configurations, thus yielding smaller matrices to diagonalize). The last step is the diagonalization. For practical purposes, the one-electron basis set is generally taken orthogonal. Our orbital choice is the set of single-particle (SP) states, i.e., the eigenfunctions of the one-electron Hamiltonian (1), which we compute by first integrating $\hat{h}_i$ using a finite differences scheme, and then diagonalizing the resulting matrices with the implicitly restarted Arnoldi iterative method.[19] Since we must select a finite basis set, the natural choice is the $M$ lowest-energy eigenvectors. Actually, in our system the lowest-energy part of the single-electron spectrum has a null ($l_z=0$) $z$-component of the angular momentum, i.e., many $s$ ($l_z=0$) SP states lie energetically below the first $p$ ($l_z=\pm1$), and higher angular momentum states are much more excited. Then, we employ a $2-n-2$ basis set in the FCI calculations, i.e., a basis set including the $n$ lowest-lying $s$ and the lowest-lying degenerate pair of $p$ orbitals (both $p_{+1}$ and $p_{-1}$ orbital pairs), these orbitals making, in all studied cases, a negligible contribution to the ground and lowest-lying excited states. In practice, we have checked that, in order to describe the low-lying energy part of the many-electron system, setting $n=10$ is more than enough (e.g., the results for the 4-electron system—both the energy and the relevant components of the low-lying eigenvectors—are almost identical employing either $n=10$ or $n=14\,s$ orbitals). With the eigenvectors obtained, we also simulate the low-lying part of the absorption spectrum. To this end, we calculate, within the dipole approximation, the $0\rightarrow K$ charge transition probability from the ground state $\Psi_0$ to the state $\Psi_K$ (both of them expressed as linear combinations of the many-electron basis set of Slater determinants $\{\Phi_i\}$). These transitions, related to the density dipole modes, preserve the spin of the system, and the corresponding transition probability is given by

$$\left|\mathbf{k}\cdot\left\langle\Psi_0\left|\sum_{i=1}^{N}\mathbf{r}_i\right|\Psi_K\right\rangle\right|^2, \tag{3}$$

where $\mathbf{k}$ is the polarization vector of the incident electromagnetic radiation.

We also simulate the spin transition probability (spin dipole modes, implying spin changes). The corresponding transition probability reads

$$\left|\mathbf{k}\cdot\left\langle\Psi_0\left|\sum_{i=1}^{N}\eta_{\sigma_i}\mathbf{r}_i\right|\Psi_K\right\rangle\right|^2, \tag{4}$$

where $\eta_\sigma=+1(-1)$ for $\sigma=\uparrow(\downarrow)$ and, as above, $\mathbf{k}$ defines polarization. For both, density and spin dipole modes, we

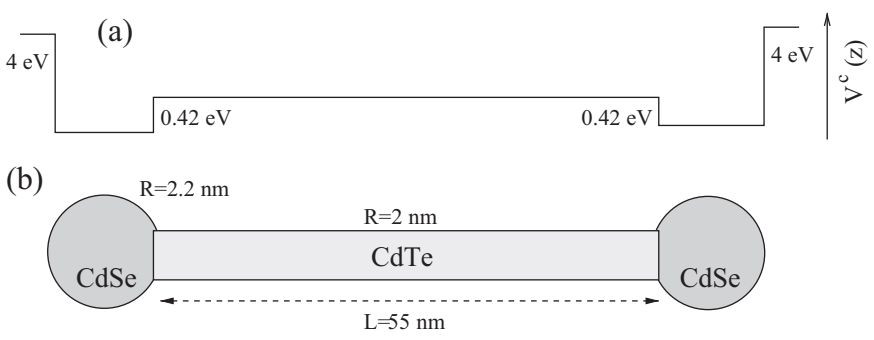


FIG. 1. (a) Schematic profile of the spatial confining potential along the $z$ axis for the nanostructures under study sketched in (b).

consider in-plane ($\mathbf{k} \perp \hat{\mathbf{z}}$) and $z$ ($\mathbf{k} \parallel \hat{\mathbf{z}}$) polarizations. The in-plane polarization transition changes the $z$-component of the total angular momentum ($\Delta L_z = \pm 1$), while $z$-polarization preserves it ($\Delta L_z = 0$). Our simulations assume a low temperature of the system ($T = 1$ K, i.e., 0.1 meV approximately). We assume the Boltzmann thermal distribution $p_i(T) = \frac{g_i}{g_0} e^{-\Delta E_i / k_B T}$ for the initial-state occupation at temperature $T$, with $g_i(g_0)$ as the degeneracy factor of the state $\Psi_i$ (ground state), $\Delta E_i$ the energy difference between $\Psi_i$ and the ground state, and $k_B$ the Boltzmann constant. We then use an intermediate normalization, i.e., the ground-state occupation is always set to one.

## III. RESULTS AND DISCUSSION

We first study the electronic structure of the ground state of CdSe/CdTe/CdSe NDs whose geometry, material parameters, and confining potential are described in Sec. II. The $z$ profiles of the lowest-lying orbitals are represented in Fig. 2. Such profiles are obtained by integrating the in-plane coordinates of the corresponding orbital. From this figure one can see that the two lowest-lying orbitals, that are quasi-degenerate, are mostly localized within the two spheres of the ND, while the more excited orbitals expand their density in the central cylinder, with a negligible density in the spheres. The preferential localization of the density along the ND can be rationalized from the orbital energies. Thus, while the energy $\varepsilon(s_1) \approx \varepsilon(s_2)$ is 0.489 eV, close to the barrier height (0.42 eV), the energy $\varepsilon(s_3) = 0.737$ eV is already much higher and, since orbitals must be orthogonal, the localization of $s_1$ and $s_2$ in the spheres pushes the rest of orbitals towards the long central cylinder, their orbital energies being close ($\varepsilon(s_4) = 0.740$ eV, $\varepsilon(s_5) = 0.744$ eV,…, $\varepsilon(s_{10}) = 0.794$ eV). As for the $p$ orbitals of possible interest, the two lowest-lying orbitals with $l_z = \pm 1$ have also their density concentrated within the spheres and have a very excited energy: $\varepsilon(p_1) \approx \varepsilon(p_2) = 0.963$ eV.[20] And, in a similar way to $s$ orbitals, also $p_i$, $i > 2$ expand their density in the central cylinder, with a negligible density in the spheres and have an orbital energy much higher than those of the two lowest-lying $p$ orbitals: $\varepsilon(p_3) = 1.218$ eV, $\varepsilon(p_4) = 1.220$ eV, $\varepsilon(p_5) = 1.225$ eV, etc. Then, the contribution of the Slater determinants that include these $p$ orbitals to the ground and low-lying many-electron states is foreseeably negligible, as the calculations confirm.

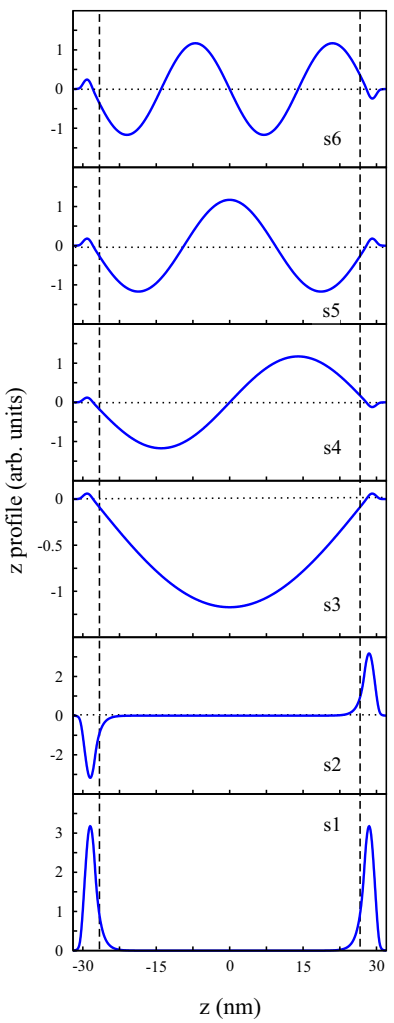


FIG. 2. $z$ profiles of the six lowest-lying $l_z = 0$ orbitals corresponding to the ND whose geometry is depicted in Fig. 1. Vertical dashed lines indicate the boundaries between the rod and the caps of the ND.

Next, we calculate the ground state of the ND populated with $N = 4$, 6, and 8 electrons by means of the FCI methodology. Several $2 - n - 2$ basis sets are employed, and the results indicate that a 2-10-2 basis set already saturates the required Hilbert space.

In the $N = 4$ case, the dominant configuration is $s_1^2 s_2^2$ with a weight larger than 99% (99.6% with the 2-10-2 basis and 99.5% with the 2-14-2 basis). This means that electronic correlation is small and that our system is in the so-called strong confinement regime, as corresponds to the electrons within the spheres. The $z$-profile of the total density and spin-up density (same as spin-down one) is represented in Fig. 3(a). It shows two strong maxima, one in each spherical cap, and a negligible density in the central cylinder, just a small penetration tail into the cylinder barrier. The integration of the density in each cap amounts to nearly 2, as corresponds to two electrons in each cap. The lack of fine details modulating the profile of the two density peaks denotes the low level of correlation between the electrons populating each cap.[14] We may refer to this configuration as a Fermi liquid phase, i.e., a system of weakly interacting particles where the kinetic energy dominates over the Coulomb repulsion.

We next increase the number of electrons in the ND up to $N = 6$. In this case, the ground state dominant configuration is $s_1^2 s_2^2 s_3^2$ with a weight of only 64%. As pointed out above, orbitals $s_1$ and $s_2$ are energetically separated from the rest of orbitals, and their electronic densities are concentrated within the spherical caps. On the other hand, $s_3$ has an orbital energy close to many other orbitals $s_i$, $i > 3$, all of them with densities concentrated within the central cylinder (see Fig. 2). The closeness of orbital energies of many orbitals $s_i$, $i > 2$, explains the relevant contributions to the ground state of many excited configurations $s_1^2 s_2^2 s_i^2$, $i > 3$ and $s_1^2 s_2^2 s_i s_j$, where either $i > 3$ or $i$ and $j > 3$, and therefore the fact of a high electronic correlation. The $z$-profile of the total density and spin-up density is represented in Fig. 3(b). It shows two strong maxima, one in each spherical cap, and additionally a pair of maxima in the central cylinder. The

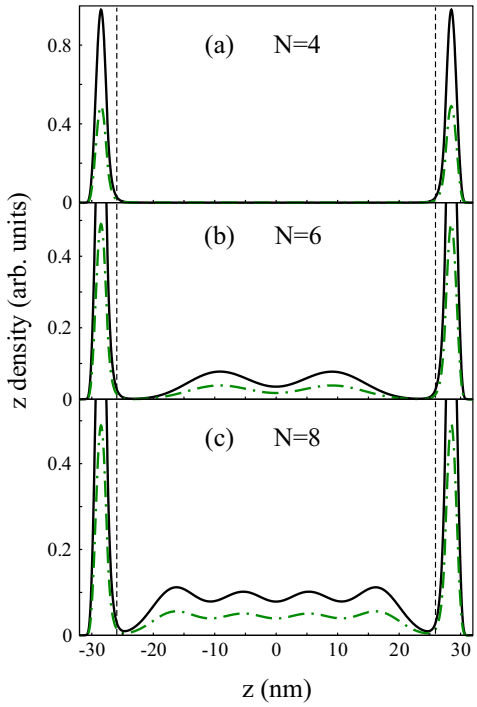


FIG. 3. (a) 4-electron ND $z$-density profiles: total density (full line) and spin-up density (dot-dashed line). The spin-down density has the same profile as the spin-up one. (b) 6-electron ND $z$-density profiles. (c) 8-electron ND $z$-density profiles. In the case of $N = 6$ and $N = 8$, the density profiles have been cut to better display spin-density-waves in the ND central region. Vertical dashed lines indicate the boundaries between the rod and the caps of the ND.

integration of the density in each cap is nearly 2, as corresponds to two electrons in each cap and two electrons in the central cylinder. Thus, while the *pair* of electrons in each cap displays a density profile with a single maximum (Fermi liquid), the *pair* in the cylinder displays a twofold maximum, as correspond to a strongly correlated Wigner crystal, i.e., a phase where the Coulomb repulsion dominates. We are thus in front of a phase with a mixed situation, i.e., a MP. In these truly three-dimensional systems, the inhomogeneous confining potential along the $z$ axis leads to the formation of a phase characterized by an uneven electronic-density distribution, in which some regions of the many-electron system behave like a Fermi liquid while, simultaneously, other more dilute regions display the typical quasi-classical Wigner distribution of the charge maxima in the electron-density profile. Due to the relatively long cylinder length, the quantum effects coming from the longitudinal confinement are negligible. Then, electron-electron interactions dominate over the kinetic energy, and a high correlation regime is achieved. In order to minimize the energy of the system, electrons localize in an ordered way, resembling quasi-classical particles along the central cylinder.

Finally, we consider the case with $N=8$ electrons. The ground state dominant configuration is now $s_1^2 s_2^2 s_3^2 s_4^2$ with a weight of only 58%, which means high correlation regime. However, as in the case of $N=6$, we are actually dealing with a MP, as is revealed by the $z$-density profiles shown in Fig. 3(c). In this case, the density profile integrates around 4 within the central cylinder and shows four maxima, while integrates around 2 in each cap, where a single maximum is displayed. The overall obtained results confirm and strengthen the previous ones obtained at the LSDFT level.[14]

We complete our study with the simulation of some absorption spectra. As stated in Sec. II, our computations assume a temperature $T=1$ K, consider in-plane and longitudinal polarizations, and include density and spin dipole modes. For axially symmetric systems, the transition probability equations (3) and (4) lead to the following selection rules: $\Delta L_z = \pm 1$ for in-plane polarization and $\Delta L_z = 0$ for longitudinal or $z$ polarization.

The in-plane polarization transitions are well defined and highly energetic. They are displayed in Fig. 4 for the case of $N=4$ and $N=6$ electrons. As we can see, the spectra of $N=4$ and $N=6$ are very similar. In the $N=4$ case, it includes a single peak at 538 meV that can be fairly described as a superposition of nearly degenerate $s_1 \rightarrow p_1$ and $s_2 \rightarrow p_2$ SP absorptions. In the $N=6$ case, the electron correlation is quite more relevant, and the orbital description is at most qualitative. However, we may say that the strong peak arising at 535 meV [see Fig. 4(b)] mainly corresponds to $s_1 \rightarrow p_1$ and $s_2 \rightarrow p_2$ SP transitions too (transitions $s_{i>2} \rightarrow p_1$ or $p_2$ are almost forbidden due to the negligible orbital overlaps associated). The second peak at 544 meV is weak and can be qualitatively ascribed to a mixture of SP transitions, involving $s_1 \rightarrow p_1$, $s_2 \rightarrow p_2$, $s_1 s_3 \rightarrow s_4 p_1$, etc. The reason for the similarity of the in-plane spectra despite the different correlation regimes of the $N=4$ and $N=6$ systems traces back to the fact that $s_1$, $s_2$, $p_1$, and $p_2$ orbitals are concentrated in the caps, while $s_i$, $i > 3$, orbitals are basically confined within the cylinder. Interestingly, the spin and charge modes are almost degenerate (see Fig. 4). It comes from the fact that configurations $s_2 p_2$ and $s_1 p_1$ are almost degenerate and that, due to the confinement of the orbitals $s_1$, $s_2$, $p_1$, and $p_2$ within the caps (see Fig. 1), the bielectronic integrals[21] $J_1=(s_1 s_1|p_1 p_1) \approx J_2=(s_2 s_2|p_2 p_2)$ and $K_1=(s_1 p_1|p_1 s_1) \approx K_2 = (s_2 p_2|p_2 s_2)$, amount almost to the same than $(s_1 s_2|p_1 p_2)$ and $(s_1 p_1|s_2 p_2)$, respectively. Then, the configurations interaction yields a quasidegeneracy of the singlet and triplet final states.[22]

The $z$-polarized spectra of $N=6$ and 8 electrons in the ND are collected in Fig. 5. These are the most interesting

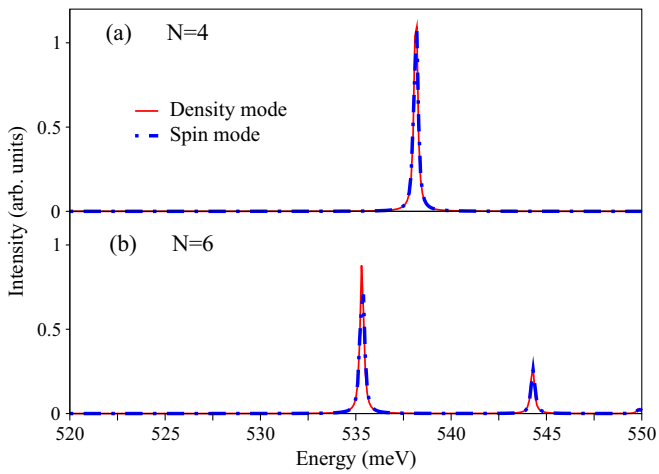


FIG. 4. Simulation of the in-plane polarized spectra for (a) $N = 4$ and (b) $N = 6$ electrons in the ND. Full (dot-dashed) lines represent density (spin) modes.

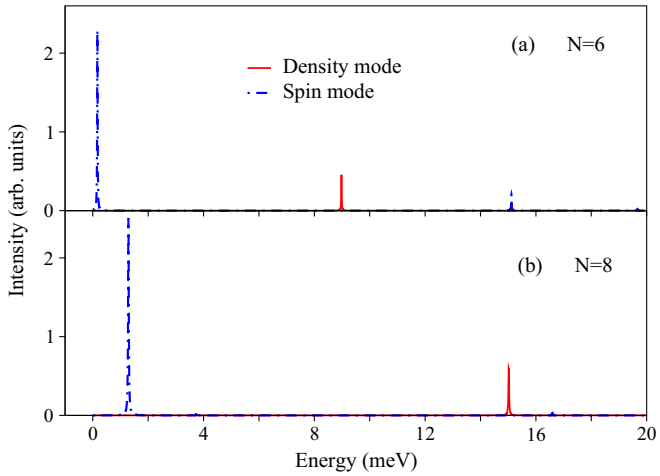


FIG. 5. Simulation of the $z$-polarized spectra corresponding to (a) $N = 6$ and (b) $N = 8$ electrons in the ND. Full (dot-dashed) lines represent density (spin) modes. An offset in the origin of the energy axis is used in order to display low-energy peaks more clearly.

modes, as far as the identification of correlation regimes is concerned. A first main difference arises between the $N=4$ system and those with $N=6$ and $N=8$. The former does not contain any visible density (nor spin) mode in the lower part of the spectrum, i.e., in the region 0-20 meV (not shown). Conversely, the other systems present a strong density mode at 9 meV ($N=6$) and 15 meV ($N=8$), and the spin counterpart mode at lower energy. In the $N=6$ system this peak corresponds to the transitions $s_3 \rightarrow s_4$, $s_3 \rightarrow s_5$, and in the $N=8$ case to the transitions like $s_4 \rightarrow s_5$, $s_3 \rightarrow s_5$, $s_3 \rightarrow s_7$. These transitions between $s$ orbitals confined in the cylinder cannot be observed in the case of the $N=4$ system because in this case $s_i, i > 2$, are empty, and the transition from $s_1$ and $s_2$ to $s_i, i > 2$, presents an almost negligible oscillator strength due to the negligible overlap of the regions where $s_1$ and $s_2$ on the one hand and $s_i, i > 2$, on the other hand present relevant electron density. As a result, the $z$-polarized absorptions observed at low energies for $N=6$ and $N=8$ can be ascribed to the presence of high correlation phases in the cylinder, the lower the transition energy the closer the involved SP states, and thus the larger the electron-electron correlation.

As a whole, the absorption spectrum reveals the signatures of both, Fermi liquid and Wigner crystal phases, turning therefore into a suitable tool to confirm the existence of mixed correlation phases in these systems.

## IV. CONCLUSIONS

In the present paper, we carry out FCI calculations of the ground and low-lying states of many electrons confined in a ND. In these many-electron diluted systems subject to inhomogeneous spatial confining potentials, we find out the existence of MPs, i.e., phases in which some regions of the many-electron system behave like a Fermi liquid while, simultaneously, other more dilute regions display the typical quasi-classical Wigner distribution of the electron density. The present results confirm and reinforce previous results obtained at the local spin-density functional theory level. Additionally, we enclose the simulations of absorption spectra, which exhibit in-plane and $z$-polarized modes that reveal the different correlation regimes occurring in these systems.

## ACKNOWLEDGMENTS

Support from MICINN projects CTQ2011-27324 and FIS2011-28617-C02-01, UJI-Bancaixa projects P1-1A2009-03 and P1-1B2011-01, and Generalitat de Catalunya Grant 2009SGR1289 is acknowledged. A.B. acknowledges the support from the Spanish FPI (MCINN) program.

[1]L. Jacak, P. Hawrylak, and A. Wójs, *Quantum Dots* (Springer, Berlin, 1998); *Semiconductor Quantum Dots*, edited by Y. Masumoto and T. Takagahara (Springer, Berlin, 2002); *Nano-Optoelectronics*, edited by M. Grundmann (Springer, Berlin, 2002); *Semiconductor Macroatoms*, edited by F. Rossi (Imperial College Press, London, 2005).
[2]S. Kan, T. Mokari, E. Rothenberg, and U. Banin, Nature Mater. **2**, 155 (2003); S. H. Kan, A. Aharoni, T. Mokari, and U. Banin, Faraday Discuss. **125**, 23 (2004).
[3]L. Li, J. Hu, W. Yang, and A. P. Alivisatos, Nano Lett. **1**, 349 (2001).
[4]X. Peng, L. Manna, W. Yang, J. Wickham, E. Scher, A. Kadavanich, and A. P. Alivisatos, Nature (London) **404**, 59 (2000).
[5]F. Shieh, A. E. Saunders, and B. A. Korgel, J. Phys. Chem. B **109**, 8538 (2005).
[6]J. E. Halpert, V. J. Porter, J. P. Zimmer, and M. G. Bawendi, J. Am. Chem. Soc. **128**, 12590 (2006).
[7]S. Geyer, V. J. Porter, J. E. Halpert, T. S. Mentzel, M. A. Kastner, and M. G. Bawendi, Phys. Rev. B **82**, 155201 (2010).
[8]E. P. Wigner, Phys. Rev. **46**, 1002 (1934).
[9]S. M. Reimann and M. Manninen, Rev. Mod. Phys. **74**, 1283 (2002).
[10]C. Yannouleas and U. Landman, Rep. Prog. Phys. **70**, 2067 (2007).
[11]B. Szafran, F. M. Peeters, S. Bednarek, T. Chwiej, and J. Adamowski, Phys. Rev. B **70**, 035401 (2004).
[12]E. J. Mueller, Phys. Rev. B **72**, 075322 (2005).
[13]J. L. Movilla, J. Planelles, and W. Jaskolski, Phys. Rev. B **73**, 035305 (2006).
[14]A. Ballester, J. M. Escartín, J. L. Movilla, M. Pi, and J. Planelles, Phys. Rev. B **82**, 115405 (2010).
[15]L. Carbone, S. Kudera, C. Giannini, G. Ciccarella, R. Cingolani, P. D. Cozzoli, and L. Manna, J. Mater. Chem. **16**, 3952 (2006).
[16]Since no specific NR (ND) environment is determined, possible polarization effects coming from the dielectric mismatch between the NR (ND) and the surrounding medium are disregarded as in Ref. 14.
[17]Ch. H. Wang, T. T. Chen, Y. F. Chen, M. L. Ho, Ch. W. Lai, and P. T. Chou, Nanotechnology **19**, 115702 (2008).
[18]See http://code.google.com/p/citool/ for more information about CITOOL computer code.
[19]R. B. Lehoucq, K. Maschhoff, D. C. Sorensen, and C. Yang, See http://www.caam.rice.edu/software/ARPACK/ for more information about arpack computer code.
[20]This energy is located in between $\epsilon(s_{18}) = 0.957$ eV and $\varepsilon(s_{19}) = 0.984$ eV.
[21]We employ here the so-called chemical notation for integrals, i.e., $(ij|kl) = \int \phi_i(1)^* \phi_j(1)(1/r_{12})\phi_k(2)^* \phi_l(2) dv$.
[22]In short, we may reason as follows: If we approximate $J_1 = J_2 = (s_1 s_2 | p_1 p_2) = J$ and $K_1 = K_2 = (s_1 p_1 | s_2 p_2) = K$, the diagonal element of the CI matrix corresponding to the spin-adapted singlet/triplet $s_2 p_2$ configuration is $\varepsilon_s + \varepsilon_p + J \pm K$. The same can be said for the spin-adapted singlet/triplet $s_1 p_1$ configuration. The admixing off-diagonal $(s_1 p_1, s_2 p_2)$ for singlet/triplet results to be $J \pm K$. Diagonalizations yield a lowest double degeneracy involving a singlet and a triplet and additionally an excited triplet and a more excited singlet. This basic idea applies to the pair of configurations of $N=4$ $(s_1^2 s_2 p_2, s_2^2 s_1 p_1)$, $N=6$ $(s_1^2 s_3^2 s_1 p_1, s_2^2 s_3^2 s_2 p_2)$, etc.